Structural Basis for the Molecular Properties of Cytochrome c_6[†]

Alexander Dikiy,[‡] Wesley Carpentier,[§] Isabel Vandenberghe,[§] Marco Borsari,[∥] Niyaz Safarov,[‡] Elena Dikaya,[‡] Jozef Van Beeumen,*[,§] and Stefano Ciurli*[,‡]

Department of Agro-Environmental Science and Technology, University of Bologna, Via Filippo Re 8, I-40127 Bologna, Italy, Laboratory for Protein Biochemistry and Protein Engineering, Gent University, 9000 Gent, Belgium, and Department of Chemistry, University of Modena, Via Campi 183, I-41100 Modena, Italy

Received July 17, 2002; Revised Manuscript Received October 9, 2002

ABSTRACT: This is a thorough biochemical, spectroscopic, electrochemical, and structural study of a cytochrome c_6 isolated from the filamentous green alga *Cladophora glomerata*. The protein sequence, elucidated using chemical and mass spectrometric techniques, features 91 amino acids and the characteristic CXXCH heme-binding motif found in *c*-type cytochromes. The protein is monomeric in both oxidation forms, thereby putting in question a functional role for protein dimerization. Direct electrochemical measurements established, for the first time, the kinetic and thermodynamic data for the redox process in a cytochrome c_6. In particular, the quasi-reversible and diffusion-controlled redox process is accompanied by negative enthalpy and entropy changes, resulting in an $E^{\circ\prime}$ value of 0.352 V at 298 K. The pH-dependent properties of the oxidized protein, detected by UV−visible, NMR, and direct cyclic voltammetry, indicate the presence of two acid−base equilibria occurring in the acidic ($pK_a = 4.5$) and alkaline regions ($pK_a = 9.0$). NMR and electronic spectra allowed the assignment of these equilibria to deprotonation of heme propionate-7 and to replacement of the axial methionine with another ligand, respectively. The 1.3 Å resolution X-ray structure of the oxidized protein, revealing a fold typical for class I cytochromes, suggests that the conserved Lys60 replaces the axial methionine at pH >9. The heme solvent accessibility is low, and no water molecules were found in the vicinity of the axial ligands of the heme Fe. A structure-based alignment of cytochromes c_6, and the direct comparison of their structures, indicate a substantial degree of identity between the tertiary structures and suggest patches involved in protein−protein interaction. In particular, the surface electrostatic potential of cytochromes c_6 features a hydrophobic region around the heme cofactor, and a backside surface rich in negative charges.

Cytochrome c_6 (cyt c_6)[1] is a water-soluble, low-spin heme-containing protein involved in the high-potential (from 0.34 to 0.39 V) electron transfer chain of oxygenic photosynthesis (for a recent review, see ref *1*). It functions by shuttling electrons between cyt b_6/f and photosystem I (PS-I) during photosynthesis in some algae and cyanobacteria (*2*, *3*). In higher plants and evolved species of algae, cyt c_6 is replaced with plastocyanin, a blue-copper protein (*4*). While some algae and cyanobacteria synthesize only either cyt c_6 or plastocyanin, others are able to produce both proteins depending on the availability of copper in the growth medium (*5*−*8*).

The structures of two cytochromes c_6 from prokaryotes, the cyanobacteria *Arthrospira maxima* (*9*) and *Synechococcus elongatus* (*10*), one from the eukaryote red alga *Porphyra yezoensis* (*11*), and three from eukaryote green algae *Scenedesmus obliquus* (*12*), *Monoraphidium braunii* (*13*−*15*), and *Chlamydomonas reinhardtii* (*16*) are now available. The latter three organisms belong to the Chlorophyceae class. In this paper, we report the amino acid sequence, the electronic and NMR spectroscopic features, the electrochemical properties, and the high-resolution X-ray structure of oxidized cyt c_6 from *Cladophora glomerata* (hereafter *Cg* cyt c_6), a green filamentous (nonunicellular) alga, belonging to the Ulvophyceae class. *C. glomerata* does not express a plastocyanin, leaving cytochrome c_6 as the only photosynthetic electron carrier in this organism (*17*). The molecular and functional properties of *Cg* cyt c_6 will be interpreted using the structural features of the protein, and discussed in

[†] S.C. acknowledges funding from MIUR-PRIN 1999 and MIUR-PRIN 2001. A.D. is a recipient of a joint CIRMMP-MIUR fellowship and of a NATO linkage grant (LST.GLG.976270). J.V.B. is indebted to the Fund for Scientific Research-Flanders for Grants 3G042298, 3GOO6896, and 3G028201 and to the "Bijzonder Onderzoeksfonds-Universiteit Gent" for Grant 1205198, each supporting different technical aspects of this work.

* To whom correspondence should be addressed. S.C.: telephone, +39-051-209-6204; fax, +39-051-209-6203; e-mail, sciurli@agrsci.unibo.it. J.V.B.: telephone, +32-9-264-5109; fax, +32-9-264-5338; e-mail, Jozef.VanBeeumen@rug.ac.be.

[‡] University of Bologna.

[§] Gent University.

[∥] University of Modena.

[1] Abbreviations: Cyt, cytochrome; NMR, nuclear magnetic resonance; *Cg* cyt c_6, *C. glomerata* cytochrome c_6; SDS−PAGE, sodium dodecyl sulfate−polyacrylamide gel electrophoresis; IEF, isoelectric focusing; TFA, trifluoroacetic acid; TR, trypsin; ND, Asp-N endoproteinase; Tris, tris(hydroxymethyl)aminomethane; TOF, time-of-flight; MES, 2-(*N*-morpholino)ethanesulfonic acid; CHES, 2-(*N*-cyclohexylamino)ethanesulfonic acid; HEPES, *N*-(2-hydroxyethyl)-piperazine-*N*′-2-ethanesulfonic acid; NOE, nuclear Overhauser effect; NOESY, nuclear Overhauser effect spectroscopy; TOCSY, total correlation spectroscopy; TPPI, time-proportional phase increment; CV, cyclic voltammetry; PGE, pyrolitic graphite edge; PEG, polyethylene glycol.

10.1021/bi026473v CCC: $22.00
Published on Web 11/21/2002

comparison with other cytochromes c_6. This study represents an attempt to provide structure-based answers to questions involving the supposed functional role of cytochrome c_6 dimerization, as well as the molecular determinants for the spectroscopic and electron transfer properties of this class of proteins.

MATERIALS AND METHODS

Protein Isolation and Biochemical Properties. *Cg* cyt c_6 was isolated and purified as previously described (*17*). The protein purity was checked by SDS−PAGE in 15% polyacrylamide gels according to the method of Laemmli (*18*). Protein bands were stained with Coomassie Brilliant Blue R250, while the presence of heme was revealed by staining with tetramethylbenzidine (*19*). Isoelectric focusing (IEF) was performed using a Multiphor Pharmacia horizontal electrophoresis cell at 25 °C and precast 7.5% acrylamide gels. The isoelectric point was determined using the Pharmacia low-pI range standards. The molecular mass of *Cg* cyt c_6 was estimated by SDS−PAGE with the Bio-Rad broad range standards. The native molecular mass was estimated by size-exclusion chromatography using the method of Andrews (*20*). This measurement was carried out for both the oxidized and reduced protein, using 1 mM ferricyanide and dithiothreitol in eluting buffer, respectively. The *Cg* cyt c_6 concentration was determined using the bicinchoninic acid method (*21*) and bovine serum albumin as a standard.

Amino Acid Sequence Determination. Ten nanomoles of native *Cg* cyt c_6 was dehemed overnight at room temperature using an equivalent amount of $HgCl_2$ in 0.1% trifluoroacetic acid (TFA) and H_2O, in the absence of urea. Heme and salts were removed from the reaction mixture, using a Vivaspin ultracentrifugation unit with a cutoff value of 5 kDa (Vivascience, Binbrook, U.K.). Cysteines were modified using 3-bromopropylamine (*22*). Internal peptides were generated by enzymatic digestions of the apocytochrome. Three nanomoles was treated with trypsin (TR, modified porcine trypsin, Promega, Madison, WI), and an additional 3 nmol was incubated with Asp-N endoproteinase (ND, Boehringer-Mannheim, Mannheim, Germany) for 3 h at 37 °C, at an enzyme/substrate ratio of 1/40, in 50 mM Tris-HCl buffer (pH 7.6) containing 1 mM $CaCl_2$. The tryptic peptide L_{70}−K_{90} was enzymatically subcleaved using Asp-N endoproteinase under the same conditions described above. The resulting peptides were separated on a PTC-C18 column (Applied Biosystems, Foster City, CA), installed on a SMART HPLC separating system (Pharmacia, Uppsala, Sweden) using gradient elution (0.1% TFA/H_2O vs 0.08% TFA/80% acetonitrile/H_2O).

Automatic Edman degradation of the uncleaved alkylated cytochrome and of two internal peptides was performed on a 476A pulsed liquid sequenator equipped with an on-line PTH-amino acid analyzer (Applied Biosystems).

Mass determinations of the native, the dehemed, and the chemically modified *Cg* cyt c_6 were performed on a nano-electrospray ionization hybrid-quadrupole-TOF mass spectrometer (Micromass, Wythenshawe, U.K.). Fragmentation spectra for de novo sequencing of internal peptides were established with the same instrument. The sequence has been deposited in the SWISS-PROT protein sequence database (accession number P83391).

Spectroscopic Studies. UV−visible spectra were recorded on a Jasco 7800 UV−visible spectrophotometer at room temperature. The pH dependence of the spectral properties of oxidized *Cg* cyt c_6 was measured using a tricomponent buffer containing MES, CHES, and HEPES (50 mM each) (MCH buffer) at different pH values. The protein was oxidized with an excess of $K_3Fe(CN)_6$ that was subsequently removed by several cycles of solvent exchange using MCH buffer at pH 7. The pH dependence was carried out by adding 10 μL of a concentrated protein sample obtained as described above to 1 mL of MCH buffer adjusted to the required pH.

NMR experiments were performed on Bruker Avance 400 and 600 MHz spectrometers operating at 400.13 and 600.13 MHz Larmor frequencies, respectively. The concentration of samples for NMR spectroscopy was 0.5−1 mM in 50 mM sodium phosphate buffer. One-dimensional NOE spectra were recorded in difference mode using previously described acquisition schemes (*23*, *24*). Recycle delays and irradiation times were 190 and 80 ms, respectively. Two-dimensional NOESY (*25*−*27*) and TOCSY (*25*, *28*, *29*) spectra were recorded with a recycle time of 500 ms. The mixing time for NOESY was 40 ms, while the spin-lock time in TOCSY was 10 ms. The recorded matrices were constituted by 2048 × 512 data points. The spectra were calibrated by assigning a shift of 4.81 ppm at 298 K at the residual water signal (*30*). All spectra were acquired in the time-proportional phase increment sensitive (TPPI) mode (*31*, *32*) using standard pulse sequences, and processed using XWINNMR Bruker software. For pH-dependent experiments, the pH of the solution was changed by adding small amounts of NaOH or HCl with rapid stirring.

Electrochemical Measurements. Cyclic voltammetry (CV) experiments were performed with a PAR 273A potentiostat/galvanostat. A 1 mm diameter pyrolitic graphite edge disk (PGE) was used as the working electrode, while a saturated calomel electrode and a 5 mm diameter Pt electrode were the reference and counter electrodes, respectively. Potentials were calibrated against the MV^{2+}/MV^{+} couple (MV is methyl viologen). All redox potentials reported in this paper are referred to the standard hydrogen electrode. The electric contact between the reference electrode and the working solution was obtained with a Vycor set. All measurements were taken under argon using a cell for a small sample volume (V = 0.5 mL), under thermostatic control. The temperature dependence measurement of $E°'$ was performed with a nonisothermal cell, in which the reference electrode was kept at constant temperature (25 °C), while the temperature of the working cell was varied (*33*, *34*). Scan rates ranged from 0.02 to 0.5 V/s. The PGE was first treated with anhydrous ethanol for 10 min and then polished with a slurry of alumina (BDH, particle size of ∼0.015 m) and water on cotton wool for 2 min. Finally, the electrode was treated in an ultrasonic pool for 10 min. NaCl (0.1 M) was used as the base electrolyte. The experiments were performed several times, and the reduction potentials were reproducible within 2 mV. For pH-dependent experiments, the pH of the solution was changed by adding small amounts of NaOH or HCl with rapid stirring. The heterogeneous electron transfer rate constant ($k°$) was determined from cyclic voltammetric peak separation as a function of scan rate (*35*).

Table 1: X-ray Data Collection Statistics and Data Reduction for *C. glomerata* Cytochrome c_6

wavelength (Å)	0.8015
resolution range (Å)	14891−1.30
R_{sym}[a]	0.053
no. of raw measurements	114176
no. of unique reflections	27067
redundancy	20.25
high-resolution bin (Å)	1.32−1.30
% completeness	98.4
% completeness in the high-resolution bin	97.6
% greater than 3σ	80.7
% greater than 2σ in the high-resolution bin	59.7
redundancy in the high-resolution bin	38.68
I/σ	25.3
I/σ in the high-resolution bin	3.6
space group	$P4_12_12$
$a = b$ (Å)	46.060
c (Å)	100.530

[a] $R_{sym} = \sum|I_i - \langle I\rangle|/\sum\langle I\rangle$, where I_i is an individual intensity measurement and $\langle I\rangle$ is the average intensity for this reflection with summation over all the data. In all sums, single measurements are excluded.

Protein Crystallization, X-ray Data Collection, and Processing. All crystals were grown at 4 °C using the hanging drop vapor diffusion method in Hampton Research 24-well Linbro plates. A 5 mg/mL protein solution (1 μL) in 20 mM Tris-HCl buffer (pH 7.6) was diluted with 1 μL of precipitant solution. The drop was equilibrated against 1 mL of precipitant solution. Screening with Hampton Crystal Screen revealed growth of well-formed needlelike crystals using 0.2 M sodium acetate, 0.1 M sodium cacodylate (pH 6.5), and 30% (w/v) PEG 8000 as the precipitant. Bulky crystals with dimensions of 0.1 mm × 0.1 mm × 0.6 mm on average were obtained after crystallization for 1−2 weeks and diffracted up to 1.85 Å at room temperature on an in-house Nonius X-ray diffractometer using a Cu Kα wavelength of 1.54078 Å. A crystal with dimensions of 0.2 mm × 0.2 mm × 0.6 mm was selected, transferred from the mother liquor to the cryobuffer (20% PEG 200 in precipitant solution), scooped up in a rayon cryoloop, and stored at 100 K. A data set, obtained at a wavelength of 0.8015 Å, was collected from this crystal at EMBL Outstation at the Deutsches Elektronen SYnchrotron (DESY) beam line X13 in Hamburg, Germany. Data were collected over a 60° range at 100 K (Oxford Cryosystem) using a 165 mm MAR CCD imaging plate scanner. The crystal diffracted satisfactorily to 1.30 Å. The data set was processed using DENZO and SCALEPACK (*36*, *37*) (Table 1).

Structure solution and refinement were carried out with programs from the CCP4 package (*38*) unless otherwise stated. Initial phases were obtained by molecular replacement [AMoRe (*39*)] using the structure of cyt c_6 from *M. braunii* (*Mb* cyt c_6, PDB entry 1CTJ) (*13*), with anisotropic data, cofactor atoms, and all water atoms omitted. Randomly selected reflections (5% of the total) were used as an R_{free} set for cross validation. The density assignment was carried out automatically with the program ARP (*40*, *41*). After incorporation of the heme cofactor, subsequent maximum likelihood-based restrained isotropic refinement cycles were carried out using the REFMAC program (*42*, *43*). Automatic solvent building was performed using the program ARP, keeping only those water molecules having a density of $>1.5\sigma$ in the $2F_o - F_c$ electron density map. When the R-factor decreased to 0.21, further refinement was carried out anisotropically to improve R and R_{free}. At an R-factor of 0.17, the positions of hydrogen atoms were calculated before each maximum likelihood refinement cycle, and their contribution to the structure factors was added to the structure factors calculated from the model. The final structure had an overall R-factor of 0.143 and an R_{free} of 0.190 (see Table 2). The stereochemistry of the final model was checked using the program PROCHECK (*44*). The refined crystallographic coordinates and structure factor amplitudes have been deposited in the Protein Data Bank (PDB entry 1LS9).

Table 2: Summary of the Crystallographic Analysis and Refinement for *C. glomerata* Cytochrome c_6

no. of protein atoms	674
no. of solvent atoms	200
no. of bound metal ions	1 Fe
temperature factor for protein atoms (Å^2)	12.90
temperature factor for solvent atoms (Å^2)	29.82
temperature factor for heme	13.09
rmsd for bond lengths (Å)	0.024
rmsd for bond angles (Å)	0.033
rmsd for planes (Å)	0.016
Ramachandran plot, most favored region (%)	85.0
Ramachandran plot, additional allowed region (%)	15.0
R-factor (R_{free})[a] (%)	14.3 (19.0)
free correlation coefficient (%)	94.6

[a] R-factor $= \sum||F_o| - |F_c||/\sum|F_o|$. R-factor and R_{free} are calculated by using the working and free reflection sets, respectively; the free reflections (5% of the total) were held aside throughout the refinement.

RESULTS

The purified *Cg* cyt c_6 migrated as a single band during SDS−PAGE, indicating the homogeneity of the purified protein. IEF experiments allowed the observation of two heme-staining bands, corresponding to the reduced and oxidized forms, with pI values of 4.3 and 4.7, respectively.

The primary structure of the protein, elucidated using a combination of chemical and mass spectrometric sequencing techniques, is shown in Chart 1, with the heme-binding residues indicated with asterisks.

The uncleaved, chemically modified apocytochrome was subjected to automated Edman degradation, which revealed the first 60 amino acid residues, including two cysteines at positions 17 and 20. Apart from a few residues, including the very last residue at the C-terminus, the remainder of the primary structure was determined by tandem mass spectrometry of the tryptic peptides. A list of the peptide masses is given in Table 3. The quality of the fragmentation spectra for the tryptic peptide TR-8 (Glu70−Lys90) and TR-9 (Gly61−Lys90) was not sufficient for determination of the residues from position 70 to 74. Five cycles of Edman degradation, performed on peptide TR-8, allowed us to identify these four residues and to assign the isoleucine at position 75. The isobaric amino acids Ile and Leu, as well as Gln and Lys, cannot be differentiated by tandem MS, and therefore, a subcleavage with N-Asp endoproteinase was performed on TR-8. Three cycles of chemical sequencing on subpeptide NDTR-1 revealed the Asp-Gln-Ala sequence stretch at positions 84−86.

Mass spectrometric analysis of the native protein yielded a value of 10 449.54 Da (Figure 1A). The spectrum of the

Chart 1

```
1         10        20        30        40        50        60        70        80        90
                  *  **                                      *
VDAELLADGKKVFAGNCAACHLGGNNSVLADKTLKKDAIEKYLEGGLTLEAIKYQVNNGKGAMPAWADREVDEDIEAVSNYVYDQAVNSKW
```

Table 3: List of Peptide Masses[a]

peptide	sequence position	experimental mass (Da)	theoretical mass (Da)
TR-4	V1−K10	1029.5	1029.5
TR-5	G61−R69	973.28	973.4
TR-6	V12−K32	2059.9	2059.9
TR-7	Y42−K53	1305.5	1305.7
TR-8	E70−K90	2386.6	2386.1
TR-9	G61−K90	3341.4	3341.5
ND-2	D84−W91	946.5	946.5
ND-3	D8−A30	2445.2	2245.1 + Hg
ND-4	D73−Y83	1286.6	1286.6
NDTR-1	D84−K90	760.5	760.4
NDTR-2	D73−Y83	1286.8	1286.1
	D74−Y83	1171.8	1171.5

[a] All theoretical values concern monoisotopic masses.

dehemed *Cg* cyt c_6 revealed a mass of 10 032.67 Da. This result, minus 200 Da for a bound Hg atom, exactly matches the calculated mass of 9833.03 Da for the apocytochrome (mercury binding to apocytochrome is often observed after $HgCl_2$ treatment to remove heme). The last residue, a tryptophan, was identified by calculating the mass difference between the experimental mass for the apocytochome and the theoretical mass for the incomplete sequence. Trp91 was confirmed by tandem MS on peptide ND-2 (Asp84−Trp91). The molecular mass estimated by SDS−PAGE and gel filtration was 9.9 kDa, indicating that the protein is a monomer in solution, regardless of the oxidation state (Figure 1B).

The 400 MHz ^{1}H NMR spectrum of oxidized *Cg* cyt c_6 at pH 5.0 is shown in Figure 2A. The spectrum is characterized by several signals shifted outside the diamagnetic region, both downfield and upfield. The analogy of the chemical shifts, line widths, and relaxation time constants T_1 and T_2 of the hyperfine-shifted signals with low-spin heme Fe(III) cytochromes with His/Met axial coordination indicated that they correspond either to protons of heme substituents or to protons of axial ligands. In particular, a strong similarity was observed with the ^{1}H NMR spectrum of oxidized cyt c_6 from *M. braunii* (*Mb* cyt c_6) (*15*), allowing us to assign most signals by analogy, as reported in Table 4. Such assignment was independently confirmed by one- and two-dimensional paramagnetic NMR spectra. A dipolar connectivity was observed between signals A and G (Figure 3A); this connectivity immediately sets these signals as being due to heme 8-CH_3 and 1-CH_3 groups, or vice versa. Further inspection of the NOE spectrum reveals a connectivity of signal A with signal C, confirmed in the NOESY spectrum (Figure 3B, cross-peak 1). Signal C, on its turn, shows a strong dipolar interaction with signal I at 9.3 ppm (cross-peak 2) and with signals J and K at 1.6 and 1.0 ppm, respectively (cross-peaks 3 and 4, respectively). Signal I is connected in a dipolar way with signals J and K, which further show a strong peak with each other (not shown). This pattern of connectivities, together with the presence of cross-peaks 5−7 connecting signal A with signals I−K, allowed us to unambiguously assign signal A to 8-CH_3, and signals

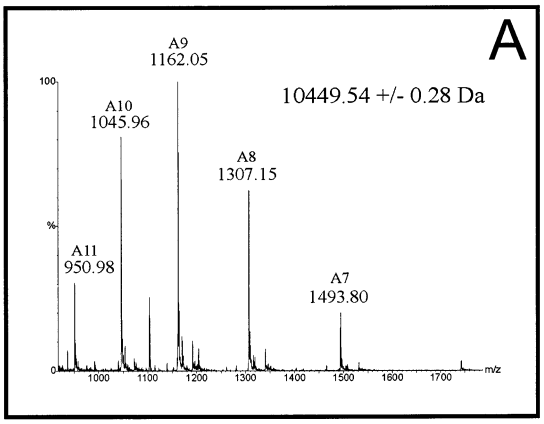

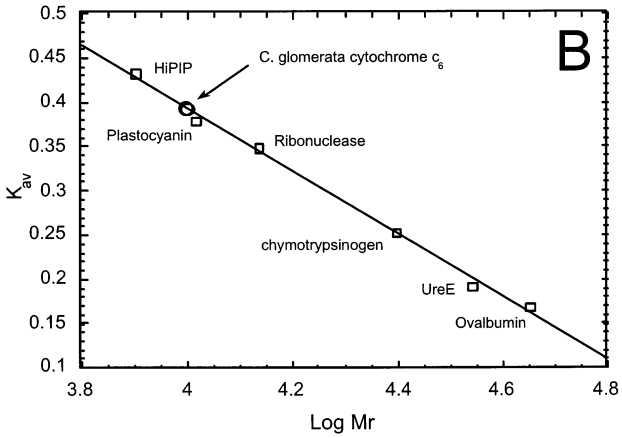

FIGURE 1: (A) Electrospray ionization spectrum of *C. glomerata* cytochrome c_6. The relative intensities of the peaks are shown against the mass/charge ratio. (B) Selectivity plot for oxidized and reduced *C. glomerata* cytochrome c_6 (○) obtained using an FPLC Superdex 75 HR 10/30 column (Pharmacia) eluted (0.5 mL/min) using 50 mM sodium phosphate buffer (pH 7.5) containing 150 mM NaCl. The proteins used as standards were ovalbumin, *Bacillus pasteurii* UreE (*78*), chymotrypsinogen, ribonuclease, *Synechocystis* PCC6803 plastocyanin (*79*), and *Rubrivivax gelatinosus* HiPIP (*80*) (45, 35, 25, 13.7, 10.5, and 8 kDa, respectively).

C and I−K to the nearby heme propionate-7 chain. The most shifted signals (C and I) are assigned to 7-Hα protons, which are closer to the Fe(III) ion, whereas signals J and K are assigned to 7-Hβ protons. Signal G is therefore associated with 1-CH_3. The assignment of signal B and F to 3-CH_3 and 5-CH_3, respectively, follows from the known fact that methyl groups situated on the opposite heme pyrrole rings in low-spin Fe(III) systems always feature similar chemical shifts (*45*). Signals D and H disappear in D_2O; on the basis of their chemical shifts and line widths, they can be assigned to exchangeable protons of the Fe(III) axial ligands. In particular, the more shifted and broader signal D can only be due to the Nδ aromatic proton of the axial histidine, while signal H is tentatively assigned to the backbone NH of the same residue. Indeed, the comparison of this assignment with the available data on *Mb* cyt c_6 supports this conclusion. In the upfield region of the spectrum, three hyperfine-shifted signals (X, Y, and Z at −8.7, −9.5, and −10.4 ppm,

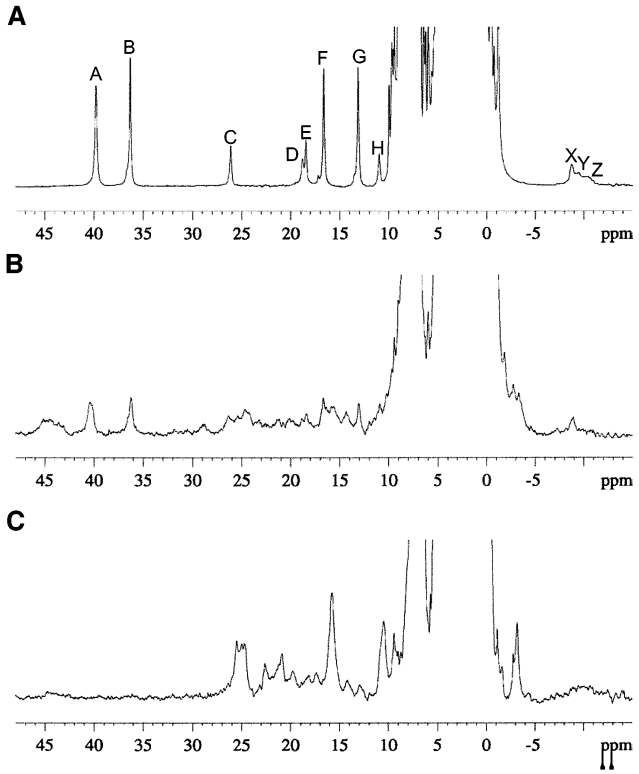

FIGURE 2: 400 MHz 298 K ^{1}H NMR spectra of oxidized *C. glomerata* cytochrome c_6 in 50 mM sodium phosphate buffer: (A) pH 5.0, (B) pH 9.0, and (C) pH 10.2. The hyperfine-shifted signals are labeled according to the text and Table 4.

Table 4: Assignment of the Hyperfine-Shifted ^{1}H NMR Signals of Oxidized *Cg* Cyt c_6 and Comparison with Those of Oxidized *Mb* Cyt c_6

signal	chemical shift for *Cg* cyt c_6 (ppm)[a]	chemical shift for *Mb* cyt c_6 (ppm)[b]	assignment
A	39.8	37.5	heme 8-CH_3
B	36.3	34.8	heme 3-CH_3
C	26.2	25.9	heme 7Hα
D	18.8	18.6	Fe−His Hδ1
E	18.5	18.0	Fe−His Hβ
F	16.6	16.4	heme 5-CH_3
G	13.3	12.8	heme 1-CH_3
H	11.0	10.3	Fe−His NH

[a] From this work; $T = 298$ K and pH 5.0. [b] From ref *15*; $T = 300$ K and pH 5.0.

respectively) are observed. They are considerably broader than the others, and feature the shortest T_1 values. These properties allowed us to tentatively assign them to protons of the axial ligands. In analogy with other *c*-type cytochromes studied by NMR, the more intense upfield-shifted signal X could be assigned to methyl protons of the Fe(III)-coordinated methionine, while signals Y and Z could be attributed to either the Hγ proton of the axial methionine or Hϵ1 of the axial histidine.

The ^{1}H NMR spectrum of *Cg* cyt c_6 undergoes pH-dependent changes. The spectra at pH 5.0, 9.0, and 10.2 are shown in panels A−C of Figure 2. In the acidic to neutral region, only modest alterations of chemical shift values for all hyperfine-shifted signals were observed, with the largest involving signal C (heme propionate 7-Hα protons). Figure 4A shows the chemical shift values for this signal as a function of pH, fitted to a theoretical one-proton dissociation equation that provides a pK_a of 4.58 ± 0.04. At pH 9 (Figure 2B), the spectrum features more drastic changes, with new signals appearing over the paramagnetic part of the spectrum, while the signals of the neutral form strongly decrease in intensity. Additionally, some broadening of the signals occurs. At strongly basic pH values (Figure 2C), the spectrum features a totally novel set of hyperfine-shifted signals. This pH-dependent behavior in the alkaline region is corroborated by the pH dependence of the Soret band in the UV−visible spectra of oxidized *Cg* cyt c_6 (Figure 4B). This figure shows pH-dependent changes in the Soret peak wavelength resulting in the determination of an evident pK_a value of 9.04 ± 0.09, as obtained from theoretical fitting of the experimental data to a one-proton ionization equilibrium equation.

Cg cyt c_6 yielded a quasi-reversible (*46*) cyclic voltammetric (CV) response on the bare PGE microelectrode (Figure 5A). The peak separation in CV experiments varied from 70 to 120 mV for scan rates in the range of 0.02−0.50 V/s. Anodic and cathodic peak currents were almost identical, and both were proportional to the protein concentration (Figure 5B) and $\upsilon^{1/2}$ (υ is the scan rate) (Figure 5C), indicating a diffusion-controlled electrochemical process. The calculated heterogeneous electron transfer rate constant, $k°$, equals $(7.6 \pm 0.8) \times 10^{-3}$ cm/s at 298 K. Given the quasi-reversibility of the electrochemical process, the symmetrical shape of the voltammograms and the almost negligible influence of the scan rate on the half-wave potentials, the $E_{1/2}$ values could confidently be assumed to represent the $E°'$ values. A reduction potential of 0.352 V at pH 7, 298 K, and 0.1 M NaCl (total ionic strength) was obtained for the cytochrome.

The cytochrome yielded a single, quasi-reversible, one-electron, and diffusion-controlled voltammetric wave in the range of 273−313 K. Using a nonisothermal cell, the standard entropy change of the reduction ($\Delta S°_{rc}$) could be calculated from the slope of the plot of $E°'$ versus temperature (*33*, *47*), while the enthalpy change ($\Delta H°_{rc}$) was obtained using the Gibbs−Helmholtz equation, namely, from the slope of the $E°'/T$ versus $1/T$ plot (Figure 5D). The thermodynamic parameters thus determined are as follows: $\Delta S°_{rc} = -48.2$ J mol^{-1} K^{-1} and $\Delta H°_{rc} = -47.2$ kJ/mol.

The pH dependence of the reduction potential was investigated to ascertain whether the ionization processes detected by NMR and electronic spectroscopies also influence the redox properties. A single quasi-reversible, one-electron, and diffusion-controlled voltammetric signal for the reduction of *Cg* cyt c_6 was observed from pH 3.5 to 7.5 on the PGE, at 293 K. Starting from the low-pH limit, the reduction potential decreased with increasing pH up to 5.5, remaining constant between pH 5.5 and 7.5, and following a titration pattern typical of an acid−base equilibrium (Scheme 1) that occurs in both redox forms of the protein.

The experimental data could be satisfactorily fitted to the following one-proton equilibrium equation (*48*):

$$E_m\,(\mathrm{mV}) = E_m(\mathrm{A}) + 2.303\frac{RT}{n\mathscr{F}}\log\left(\frac{[H^+] + K_R}{[H^+] + K_O}\right) \quad (1)$$

providing the following values: p$K_O = 4.2$, p$K_R = 4.4$, $E°$-(A) = 0.368 V, and $E°$(B) = 0.355 V (Figure 4C). Outside the pH range of 3.5−7.5, the voltammetric response dramati-

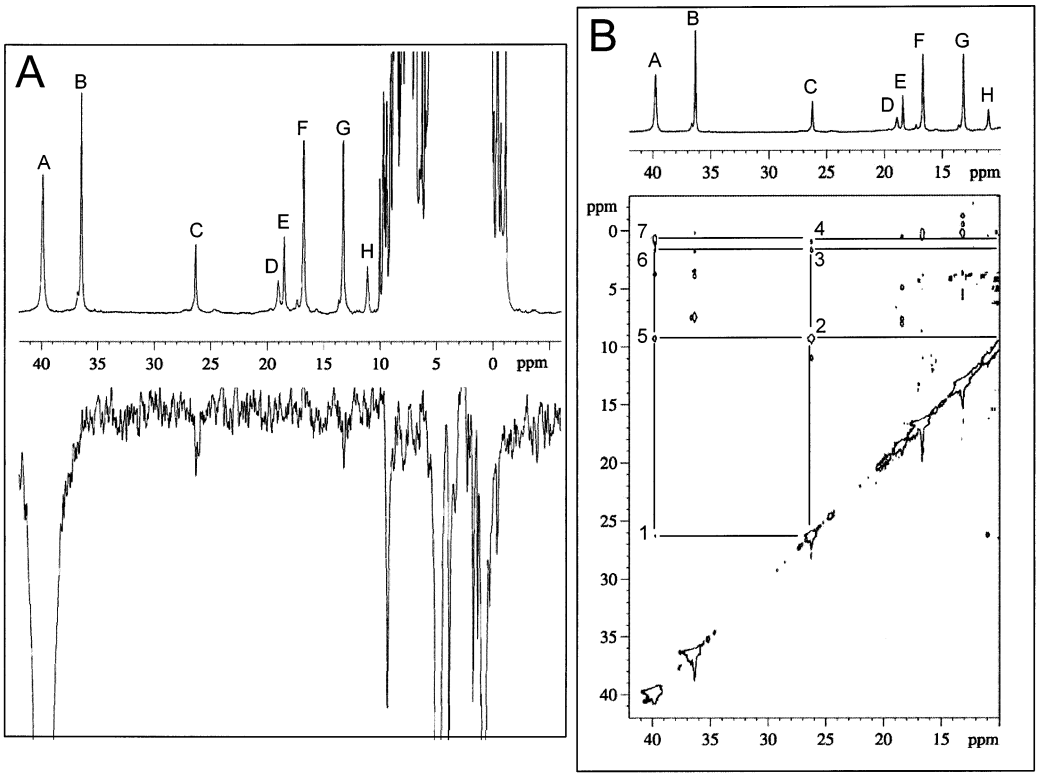

FIGURE 3: 600 MHz 298 K ^{1}H NMR spectra of oxidized *C. glomerata* cytochrome c_6 in 50 mM sodium phosphate buffer (pH 6.5): (A) one-dimensional NOE spectrum obtained upon saturation of signal A and (B) two-dimensional NOESY spectrum. See the text for signal and cross-peak assignment.

cally worsened, with the CV peaks broadening and decreasing in intensity. The heterogeneous redox process was no longer diffusion-controlled, with the peak current not showing a linear dependence on $v^{1/2}$ but rather on v.

The crystal structure of *Cg* cyt c_6 was determined by molecular replacement using the available structural data for *Mb* cyt c_6 [PDB entry 1CTJ (*13*)]. A single molecule of protein (10.5 kDa) is present in the asymmetric unit, resulting in a volume-to-mass ratio V_M of 2.54 Å^3/Da and a solvent content of 51.18%. The structure of *Cg* cyt c_6, determined at high resolution and with good statistics (Tables 1 and 2), is shown in Figure 6A, and reveals the characteristic fold of class I cytochromes. The N-terminal helix (helix I) is from Ala3 to Asn16, is bent at Cys17, and further continues to Gly24. The latter three residues (Leu22−Gly24) represent a 3_{10} helix fragment. Residues Asn25−Lys35 constitute the so-called Ω-loop, which separates the N-terminal helix from helix II (Lys36−Tyr42). The protein does not have a regular secondary structure in the region between Leu43 and Thr48. Helix III spans the Leu49−Asn58 region and is followed by a very short region of antiparallel β-sheet constituted by two residues (Lys60 and Met63), sustained by a hydrogen bond between the amide proton of Lys60 and the carbonyl atom of Met63. The Pro64−Asp71 protein region lacks any element of regular secondary structure. The protein ends by a long C-terminal helix IV from Glu72 to Val87, inserted between helices I and III, almost perpendicular to helix I and roughly parallel with helix III. The contact of helices I and IV occurs only through a single hydrophobic interaction between Gly9 (on helix I) and Ala77 and Val78 (on helix III), while helices III and IV are held together by several hydrophobic contacts and a salt bridge between the side chains of Lys53 and Glu76.

The electron density for the heme moiety is well-defined (Figure 6B). The heme is located in a hydrophobic pocket, bound to the rest of the protein through Cys17 and Cys20 (thioether links), and His21 and Met63 (axial ligands). In analogy with other *c*-type cytochromes, *Cg* cyt c_6 reveals a hydrogen bond between NHδ1 of the axial histidine and the carbonyl oxygen of Asn25. This bond is considered to be important for imposing the position of the histidine ring with respect to the heme plane.

The heme is solvent-protected, and the heme groups which are mostly accessible are 3-CH_3 and 4-CH_3 of pyrrole ring C, together with the oxygen atoms of propionate-6 (ring D) and -7 (ring A). A network of three H-bonded solvent molecules (Wat4, Wat21, and Wat27) is present around the heme propionate groups. Wat21 is placed between propionates-6 and -7 and is involved in hydrogen bonds with both propionates as well as with the NH_2 group of Gln55. No other hydrogen bonds are observed for propionate-7, while the carboxylate group of propionate-6 is further H-bound to Wat4, Wat27, and the Nζ atom of Lys60. No water molecules are found in the vicinity of the heme axial ligands.

DISCUSSION

A low-spin cyt c_6 was isolated from the green alga *C. glomerata*. This cytochrome was characterized by mass spectrometry, sequence analysis, and UV−visible and NMR spectroscopy. The sequence of *Cg* cyt c_6 reveals that the protein contains 91 amino acids and the characteristic CXXCH heme-binding motif found in *c*-type cytochromes. The presence of a minimal necessary set of the heme *c* ligand residues unambiguously identifies the amino acids directly bound to the heme moiety as Cys17, Cys20, His21, and Met63.

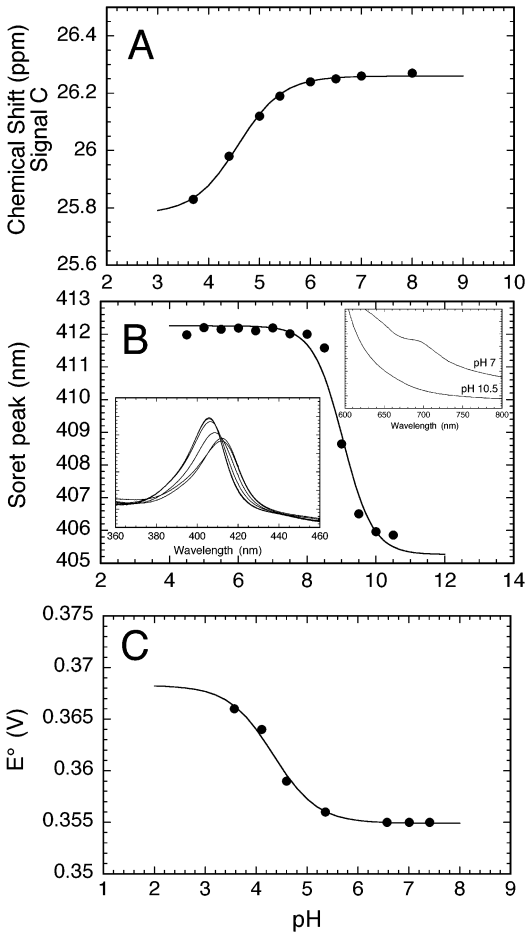

FIGURE 4: pH-dependent properties observed for *C. glomerata* cytochrome c_6 in 50 mM sodium phosphate buffer. (A) ^{1}H NMR chemical shift for signal C (heme propionate-7 Hα). (B) Soret peak wavelength in the UV−visible spectrum. The upper inset shows the disappearance of the 695 nm band at alkaline pH. The lower inset reports the Soret band as a function of pH (4.5, 7.0, 9.0, 9.5, and 10.5); the band is progressively blue-shifted as the pH increases above pH 7. (C) Electrochemical reduction potential. The fits to the theoretical one-proton acid−base equilibria are shown with solid lines.

Scheme 1: Equilibria that Exist during pH-Dependent Redox Processes Involving *C. glomerata* Cytochrome c_6[a]

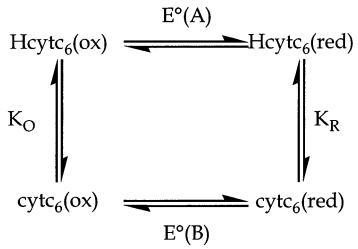

[a] $E°$(A) and $E°$(B) are the limit $E°$ values for the protein in the completely protonated and deprotonated forms, respectively, while K_O and K_R are the proton dissociation constants for the oxidized and reduced protein, respectively.

The ^{1}H NMR spectrum of oxidized *Cg* cyt c_6 is similar to that reported for *Mb* cyt c_6 (*15*, *49*), indicating an analogous electronic structure of the heme prosthetic group and, consequently, a structurally similar coordination environment for the heme Fe(III) ion. The $E°'$ value of *Cg* cyt c_6 at neutral pH (0.352 V) is essentially identical to that observed for *Mb* cyt c_6 (0.358 V) (*49*). The dependence of the reduction potential of *Cg* cyt c_6 on temperature, the first one available for this class of cytochromes, reveals that the reduction of *Cg* cyt c_6 is accompanied by negative enthalpy ($\Delta H°'$) and entropy ($\Delta S°'$) changes. This behavior has been observed for all class I cytochromes (*50*−*54*). $\Delta H°'$ is mainly the result of stabilization of the reduced state due to the ligand interactions, the hydrophobic environment at the heme−protein interface, and the limited accessibility of the heme to the solvent (*52*, *55*). On the other hand, $\Delta S°'$ is likely to be related to differences in solvation properties between the two redox states (*56*, *57*), in turn related to heme solvent accessibility (*58*). A larger conformational flexibility of the oxidized versus the reduced form has also been proposed to be the cause for the negative value of the reduction entropy (*55*, *59*, *60*). The $\Delta S°'$ and $\Delta H°'$ values for *Cg* cyt c_6 are less negative than those for cytochromes c_2 from bacteria, but more negative than those from higher plants (*52*, *54*).

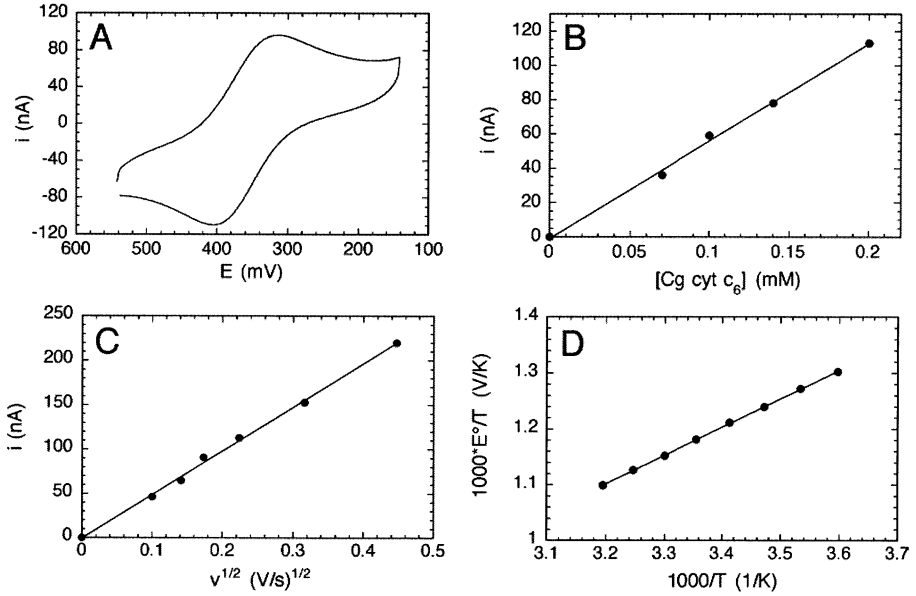

FIGURE 5: Electrochemical data for *C. glomerata* cytochrome c_6. (A) cyclic voltammogram (υ = 0.02 V/s), (B) dependence of the peak current on the protein concentration, (C) dependence of the peak current on the scan rate ($\upsilon^{1/2}$), and (D) dependence of the protein reduction potential on temperature ($E°'/T$ vs $1/T$).

Chart 2: Structure-Based Alignment among the Crystallographically Characterized Cytochromes c_6[a]

```
1LS9_Cgl     1  VDAELLADGKKVFAGNCAACHLGGNNSVLADKTLKKDAIEKYLEGGL--TLEAIKYQVNNGKGAMPAWADRLDEDDIEAVSNYVYDQAVNSKW
1C6R_Sob     2    ADLALGKQTFEANCAACHAGGNNSVIPDHTLRKAAMEQFLQGGF--NLEAITYQVENGKGAMPAWSGTLDDDEIAAVAAYVYDQASGDKW
1CTJ_Mbr     1   EADLALGKAVFDGNCAACHAGGGNNVIPDHTLQKAAIEQFLDGGF--NIEAIVYQIENGKGAMPAWDGRLDEDEIAGVAAYVYDQAAGNKW
1CYJ_Cre     1    ADLALGAQVFNGNCAACHMGGRNSVMPEKTLDKAALEQYLDGGF--KVESIIYQVENGKGAMPAWADRLSEEEIQAVAEYVFKQATDAAWKY
1F1F_Ama     2     DVAAGASVFSANCAACHMGGRNVIVANKTLSKSDLAKYLKGFDDDAVAAVAYQVTNGKNAMPGFNGRLSPLQIEDVAAYVVDQAEKG-W
1GDV_Pye     1    ADLDNGEKVFSANCAACHAGGNNAIMPDKTLKKDVLEANS----MNTIDAITYQVQNGKNAMPAFGGRLVDEDIEDAANYVLSQSEKG-W
```

[a] The regular and 3_{10}-helices are shown in yellow and purple, respectively, while asterisks and periods represent strictly conserved and conservatively substituted residues, respectively.

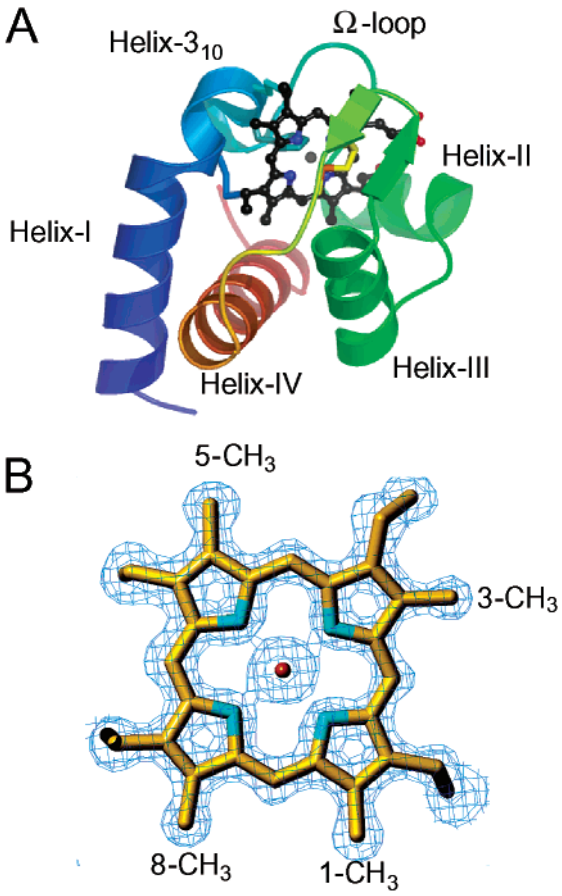

FIGURE 6: (A) Ribbon plot of oxidized *C. glomerata* cytochrome c_6, showing the secondary structure elements and the heme moiety. (B) Electron density map of the heme moiety.

The differences in redox parameters among these cytochrome families are not dramatic, indicating that the determinants of the enthalpy and entropy values are of the same type, but modulated in a different manner by the different structures. In particular, it has been proposed that entropic effects are responsible for the large differences observed between the high-potential and the low-potential *c*-type cytochromes, while enthalpic effects regulate the small potential differences that have been detected (*58*). The value determined for the heterogeneous electron transfer rate constant, $k°$, again the first one available for this class of cytochromes, is similar to those found at the same temperature for horse heart cytochrome *c* at chemically modified electrodes (*50*, *61*). A reasonable assumption for this behavior is that the factor controlling the $k°$ value is a rate-determining conformational change of the cytochrome, independent of the characteristics of the electrode itself. The value determined for $k°$ sets a lower limit for the self-exchange electron transfer occurring in solution between the two redox forms of the protein (*62*).

Cg cyt c_6 undergoes at least two proton ionization equilibria, as shown by UV−visible and NMR spectroscopies, as well as by electrochemical measurements. A first equilibrium was monitored by NMR spectroscopy and electrochemistry, providing a pK_a value of ~4.5. This process can be attributed to an ionization occurring without modifying the heme ligation state of the protein. In fact, this equilibrium results in only modest changes in ^{1}H NMR spectra (Figure 4A), very small shifts of the electrochemical potential (Figure 4C), and essential invariance of the main features of the Soret band in the visible spectrum (inset of Figure 4B). According to NMR spectroscopy, in this pH range the largest pH-dependent changes among the hyperfine-shifted signals are displayed by signal C, which corresponds to the heme propionate-7 Hα proton. On the basis of this observation, the pK_a of ca. 4.5 can be attributed to ionization of propionate-7. A spectral investigation of the pH-dependent properties of *Mb* cyt c_6 (*49*) has shown the presence of an equilibrium involving a transition between two forms of *Mb* cyt c_6, with a pK_a of 5, but the molecular basis for this equilibrium was not provided. This study suggests that this protonation equilibrium, occurring for cytochromes c_6 with a pK_a of ca. 5, generally involves heme propionate-7.

The second detected pK_a value, occurring in the alkaline region, can best be obtained from the analysis of UV−visible spectra at different pHs, which provides a pK_a value of 9.0. The electronic spectra indicate that the protein is stable at high pH, with the observed changes being reversible, and also that no autoreduction occurs at these extreme conditions. These spectra also provide valuable information concerning the nature of the observed process. The disappearance, upon changing the pH from 7 to 10.5, of the low-intensity band at 695 nm generally ascribed to an Fe(III)−SMet axial coordination (inset in Figure 4B), indicates that the axial methionine is either substituted with another ligand or detached, leaving a pentacoordinate high-spin ($S = {}^5/_2$) Fe(III) ion. The latter possibility can be ruled out on the basis of the modest changes observed in the Soret band line width and peak position (inset in Figure 4B), as well as by the absence, in the ^{1}H NMR spectra at alkaline pH, of the typical strongly shifted and broadened signals observed for high-spin Fe(III) heme systems (Figure 2B,C). All this experimental evidence is therefore consistent with the presence of an equilibrium process that involves substitution, at pH >9, of Met63, bound to Fe(III) in the acidic to neutral pH range. The slow heterogeneous electron transfer observed by cyclic voltammetry in the alkaline region could be explained by a large reorganizational energy correlated with this ligand exchange, leading to sluggish kinetics and the concomitant lack of direct electrochemical reversibility.[2] The NMR spectra recorded in the pH range of 8−10 reveal the

Table 5: Sequence Identity Values (%, lower part) and Backbone rmsd Values (Å, Upper Part) for the Crystallographically Characterized Cytochromes c_6[a]

	1LS9 Cglo	1C6R Sobl	1CTJ Mbra	1CYJ Crei	1F1F Amax	1GDV Pyez
1LS9 Cglo	−	0.48	0.67	0.68	0.80	0.85
1C6R Sobl	59.3	−	0.56	0.52	0.90	0.90
1CTJ Mbra	61.5	77.5	−	0.58	0.90	0.82
1CYJ Crei	58.1	63.3	63.7	−	0.81	0.96
1F1F Amax	53.3	46.6	46.1	49.5	−	0.82
1GDV Pyez	50.5	51.1	47.2	47.8	50.6	−

[a] 1LS9_Cglo, *C. glomerata* cyt c_6 (PDB entry 1LS9); 1C6R_Sobl, *S. obliquus* cyt c_6 (PDB entry 1C6R); 1CTJ_Mbra, *M. braunii* cyt c_6 (PDB entry 1CTJ); 1CYJ_Crei, *Ch. reinhardtii* cyt c_6 (PDB entry 1CYJ); 1F1F_Amax, *A. maxima* cyt c_6 (PDB entry 1F1F); 1GDV_Pyez, *P. yezoensis* cyt c_6 (PDB entry 1GDV).

contemporary existence of signals belonging to the acidic as well as alkaline forms of the cytochrome (Figure 2B), together with signal broadening. This could be explained only by invoking a dynamic process occurring near the intermediate exchange regime on the NMR time scale and involving two different low-spin cytochrome forms featuring different axial ligands.

Methionine exchange at high pH has been observed for several *c*-type cytochromes, and it has often been ascribed, as in this study, to an equilibrium occurring with the replacement of the axial methionine with another ligand (*49*, *59*, *63*). It has also been proposed that the latter is a lysine residue residing in a position that is appropriate for replacing the detached methionine (58, *64*, *65*). The structure of *Cg* cyt c_6 reveals the presence of a lysine residue (Lys60) in the proximity of the heme face involved with the Fe−S(Met63) bond. This lysine forms a short β-sheet with Met63, and an H-bond between its terminal amino group and the carboxylate oxygen of heme propionate-6, as well as with a group of well-defined water molecules. The pK_a for the process of methionine exchange (9.0) is fully consistent with its assignment as the deprotonation of the NH_3^+-terminal group of Lys60, which renders its neutral amino group available for coordination to Fe(III). This lysine residue is fully conserved among all cytochromes c_6 (see Chart 2), and we propose here that this process is characteristic for this class of proteins.

The percentage sequence homology is reported in Table 5. The latter also reports the overall backbone rmsd for pairs of different proteins. The backbone rmsd per residue is low (ca. 0.4 Å) in the regions encompassing helix I, the 3_{10}-helix, the Ω-loop, helix III, and helix IV, while larger differences (up to 2.5 Å) are observed for helix II and the loop connecting it to helix III. The observed trend of rmsd per residue correlates well with the sequence homology along the chain. Of the three structural features surrounding the heme group, only the Ω-loop and the loop connecting helix III to helix IV are highly conserved. These secondary structure elements are located near the solvent-exposed heme edge, around the 3-CH_3 and 4-CH_3 atoms of pyrrole ring C, suggesting that they are involved in protein−protein interactions and subsequent electron transfer through the indicated heme atoms. This type of analysis also suggests that helix II is not functionally relevant. Indeed, these conclusions are fully consistent with the recently modeled

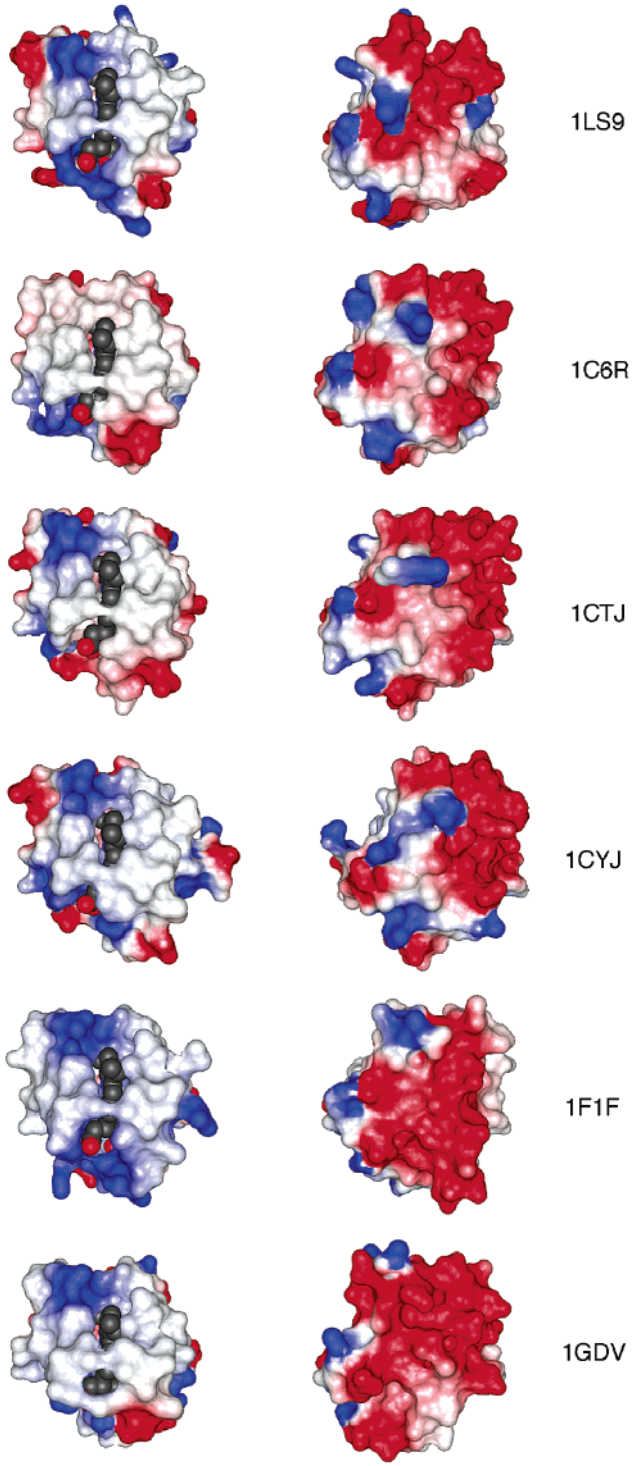

FIGURE 7: Surface potential maps for cytochromes c_6 from various sources. Two orientations, related by a 180° rotation along a vertical axis, are shown for all proteins. The heme moieties are displayed as CPK spheres. The PDB entries for all structures are shown on the right-hand side: *C. glomerata* cyt c_6 (1LS9), *S. obliquus* cyt c_6 (1C6R), *M. braunii* cyt c_6 (1CTJ), *Ch. reinhardtii* cyt c_6 (1CYJ), *A. maxima* cyt c_6 (1F1F), and *P. yezoensis* cyt c_6 (1GDV). This figure was prepared with MOLMOL, using the default parameters for electrostatic calculations (*81*).

[2] An alternative hypothesis for explaining the irreversible CV curves would involve a progressively hindered reorientation of the negatively charged protein on the negatively charged electrode surface, as the pH increases. This process, however, would result in diffusion-controlled kinetics, in contrast with the experimental observation.

structure of a complex between cyt c_6 and cyt *f* (PDB entry 1JX8).

Several structural analyses of eukaryote *c*-type cytochromes have evidenced the existence of conserved water molecules in the vicinity of the axial ligands of the heme moiety (*66*−*70*). The hydrogen bonds formed by these water molecules can determine the coordination peculiarities of the Fe ion, consequently playing a functional role in electron transfer processes. In contrast, no water molecules in position to affect Fe coordination properties, and therefore to tune its reduction potential, were found in *Cg* cyt c_6, consistent with all other structures of cytochromes c_6. This finding is in contrast with a generalized functional role of solvent molecules in eukaryotic *c*-type cytochromes.

To elucidate the possible properties of the molecular surface responsible for protein function, a comparison of surface potential maps, shown in Figure 7, was carried out. Generally, this comparison reveals a similar charge distribution among all crystallographically characterized cytochromes c_6. In particular, in all cases the surface surrounding the heme group reveals a distinct hydrophobic area, while most negative charges are located on the opposite side of the exposed heme edge. However, some subtle alterations in the charge distribution can be noticed among the analyzed proteins. A similar charge distribution has been observed in cyt c_{552} from thermophiles (*71*, *72*) and cyt c_{553} from alkalophiles (*58*). In contrast, a positively charged front surface, formed by several lysine residues grouped around the solvent-exposed edge of heme pyrrole C, is found in cyt *c* and c_2 (*73*−*76*), as well as in *Desulfovibrio vulgaris* cyt c_{553} (*77*). The surface area surrounding the heme crevice is generally considered to represent the site for molecular recognition during electron transfer. Figure 7 also shows that the heme solvent accessibility in all these proteins is very similar.

This study reveals that *Cg* cyt c_6 is monomeric in both oxidation forms in solution, and monomeric in the crystal. This observation is at variance with the results for other cytochromes c_6 found to dimerize in solution and/or in the solid state (*9*, *12*, *16*). The structural analysis performed here has further evidenced that all cytochromes c_6 have very similar primary, secondary, and tertiary structures, ruling out the possibility that these factors affect the dimerization of the proteins. Therefore, the observed differences in the oligomerization equilibria in the various cytochromes c_6 may be determined by the subtle differences in the surface electrostatic potential properties highlighted in Figure 7. Such a finding erodes the support for a generalized functionally significant oligomerization process.

To further ascertain the structural determinants of the redox-dependent functional properties of *Cg* cyt c_6, we are currently working toward the determination of the structure of the reduced form of the protein, by both NMR and X-ray crystallography.

REFERENCES

1. Reuter, W., and Wiegand, G. (2001) in *Handbook of metalloproteins* (Messerschmidt, A., Huber, R., Wieghardt, K., and Poulos, T., Eds.) pp 87−99, Wiley, New York.
2. Kallas, T. (1994) in *Molecular biology of cyanobacteria* (Bryant, D. A., Ed.) pp 259−317, Kluwer Academic Publishers, Dordrecht, The Netherlands.
3. Golbeck, J. H. (1994) in *The molecular biology of cyanobacteria* (Bryant, D. A., Ed.) pp 319−360, Kluwer Academic Publishers, Dordrecht, The Netherlands.
4. Wood, P. M. (1978) *Eur. J. Biochem. 87*, 9−19.
5. Sandmann, G., Reck, H., Kessler, E., and Boger, P. (1983) *Arch. Microbiol. 134*, 23−27.
6. Ho, K. K., and Krogmann, D. W. (1984) *Biochim. Biophys. Acta 766*, 310−316.
7. Bryant, D. A. (1994) *The molecular biology of cyanobacteria*, Kluwer, Dordrecht, The Netherlands.
8. Hill, K. L., and Merchant, S. (1995) *EMBO J. 14*, 857−865.
9. Sawaya, M. R., Krogmann, D. W., Serag, A., Ho, K. K., Yeates, T. O., and Kerfeld, C. A. (2001) *Biochemistry 40*, 9215−9225.
10. Beissinger, M., Sticht, H., Sutter, M., Ejchart, A., Haehnel, W., and Rosch, P. (1998) *EMBO J. 17*, 27−36.
11. Yamada, S., Park, S.-Y., Shimizu, H., Koshizuka, Y., Kadokura, K., Satoh, T., Suruga, K., Ogawa, M., Isogai, Y., Nisho, T., Shiro, Y., and Oku, T. (2000) *Acta Crystallogr. D56*, 1577−1582.
12. Schneckenberg, J., Than, M. E., Mann, K., Wiegand, G., Huber, R., and Reuter, W. (1999) *J. Mol. Biol. 290*, 1019−1030.
13. Frazao, C., Soares, C. M., Carrondo, M. A., Pohl, E., Dauter, Z., Wilson, K. S., Hervas, M., Navarro, J. A., De la Rosa, M. A., and Sheldrick, G. (1995) *Structure 3*, 1159−1169.
14. Banci, L., Bertini, I., Quacquarini, G., Walter, O., Diaz, A., Hervas, M., and De la Rosa, M. A. (1996) *J. Biol. Inorg. Chem. 1*, 330−340.
15. Banci, L., Bertini, I., De la Rosa, M. A., Koulougliotis, D., Navarro, J. A., and Walter, O. (1998) *Biochemistry 37*, 4831−4843.
16. Kerfeld, C. A., Anwar, H. P., Interrante, R., Merchant, S., and Yeates, T. O. (1995) *J. Mol. Biol. 250*, 627−647.
17. Safarov, N., Agalarov, R. I., Isaev, M. N., Dikiy, A., and Gasanov, R. A. (1998) in *Progress in Botanical Research* (Tsekos, I., and Moustakas, M., Eds.) pp 235−238, Kluwer Academic Publishers, Dordrecht, The Netherlands.
18. Laemmli, U. K. (1970) *Nature 227*, 680−685.
19. Thomas, P. E., Ryan, D., and Levin, W. (1976) *Anal. Biochem. 75*, 168−176.
20. Andrews, P. (1964) *Biochem. J. 91*, 222−233.
21. Smith, P. K., Krohn, R. I., Hermanson, G. T., Mallia, A. K., Garther, F. H., Provenzano, M. D., Fujimoto, E. K., Goeke, N. M., Olson, B. J., and Klenk, D. C. (1985) *Anal. Biochem. 150*, 76−85.
22. Jue, R. A., and Hale, E. J. (1994) in *Techniques in Protein Chemistry* (Crabb, J. W., Ed.) pp 179−188, Academic Press, San Diego.
23. Banci, L., Bertini, I., Luchinat, C., Piccioli, M., Scozzafava, A., and Turano, P. (1989) *Inorg. Chem. 28*, 4650−4656.
24. Dugad, L. B., La Mar, G. N., Banci, L., and Bertini, I. (1990) *Biochemistry 29*, 2263−2271.
25. Braunschweiler, L., and Ernst, R. R. (1983) *J. Magn. Reson. 53*, 521−528.
26. Macura, S., and Ernst, R. R. (1980) *Mol. Phys. 41*, 95.
27. Wider, G., Macura, S., Kumar, A., Ernst, R. R., and Wuthrich, K. (1984) *J. Magn. Reson. 56*, 207−234.
28. Davis, D. G., and Bax, A. (1985) *J. Am. Chem. Soc. 107*, 2820−2821.
29. Griesinger, C., Otting, G., Wuthrich, K., and Ernst, R. R. (1988) *J. Am. Chem. Soc. 110*, 7870−7872.
30. Bertini, I., Ciurli, S., Dikiy, A., and Luchinat, C. (1993) *J. Am. Chem. Soc. 115*, 12020−12028.
31. Marion, D., and Wuthrich, K. (1983) *Biochem. Biophys. Res. Commun. 113*, 967−974.
32. Marion, D., Driscoll, P. C., Kay, L. E., Wingfield, P. t., Bax, A., Gronenborn, A. M., and Clore, G. M. (1989) *Biochemistry 28*, 6150−6156.
33. Yee, E. L., Cave, R. J., Guyer, K. L., Tyma, P. D., and Weaver, M. J. (1979) *J. Am. Chem. Soc. 101*, 1131−1137.
34. Yee, E. L., and Weaver, M. J. (1980) *Inorg. Chem. 19*, 1077−1087.
35. Nicholson, R. S. (1965) *Anal. Chem. 37*, 1351−1355.
36. Otwinowski, Z. (1993) in *Proceedings of the CCP4 Study Weekend* (Sawyer, L., Isaac, N., and Bailey, S., Eds.) pp 56−62, Daresbury Laboratory, Warrington, U.K.
37. Otwinowski, Z., and Minor, W. (1997) *Methods Enzymol. 276*, 307−325.
38. Collaborative Computational Project, No. 4 (1994) *Acta Crystallogr. D50*, 760−763.
39. Navaza, J. (1994) *Acta Crystallogr. A50*, 157−163.

40. Lamzin, V. S., and Wilson, K. S. (1997) *Methods Enzymol. 277*, 269−305.
41. Perrakis, A., Morris, R., and Lamzin, V. S. (1999) *Nat. Struct. Biol. 6*, 458−463.
42. Murshudov, G. N., Vagin, A. A., and Dodson, E. J. (1997) *Acta Crystallogr. D53*, 240−255.
43. Murshudov, G. N., Vagin, A. A., Lebedev, A., Wilson, K. S., and Dodson, E. J. (1999) *Acta Crystallogr. D55*, 247−255.
44. Laskowski, R. A., MacArthur, M. W., Moss, D. S., and Thornton, J. M. (1993) *J. Appl. Crystallogr. 26*, 283−291.
45. Banci, L., Bertini, I., Luchinat, C., Pierattelli, R., Shokhirev, N. V., and Walker, F. A. (1998) *J. Am. Chem. Soc. 120*, 8472−8479.
46. Bard, A. J., and Faulkner, L. R. (1980) *Electrochemical methods. Fundamentals and applications*, Wiley, New York.
47. Taniguchi, V. T., Sailasuta-Scott, N., Anson, F. C., and Gray, H. B. (1980) *Pure Appl. Chem. 52*, 2275−2281.
48. Dutton, P. L. (1978) *Methods Enzymol. 54*, 411−435.
49. Campos, A. P., Aguiar, A. P., Hervas, M., Regalla, M., Navarro, J. A., Ortega, J. M., Xavier, A. V., De la Rosa, M. A., and Teixeira, M. (1993) *Eur. J. Biochem. 216*, 329−341.
50. Taniguchi, I., Funatsu, T., Iseki, M., Yamaguchi, H., and Yasukouchi, K. (1985) *J. Electroanal. Chem. 193*, 295−302.
51. Bertrand, P., Mbarki, O., Asso, M., Blanchard, L., Guerlesquen, F., and Tegoni, M. (1995) *Biochemistry 34*, 11071−11079.
52. Battistuzzi, G., Borsari, M., Sola, M., and Francia, F. (1997) *Biochemistry 36*, 16247−16258.
53. Feinberg, B. A., Petro, L., Hock, G., Qin, W., and Margoliash, E. (1998) *J. Pharm. Biomed. Anal. 19*, 115−125.
54. Battistuzzi, G., Borsari, M., Cowan, J. A., Eicken, C., Loschi, L., and Sola, M. (1999) *Biochemistry 38*, 5553−5562.
55. Battistuzzi, G., Borsari, M., and Sola, M. (2001) *Eur. J. Inorg. Chem.*, 2989−3004.
56. Cohen, D. S., and Pielak, G. J. (1995) *J. Am. Chem. Soc. 117*, 1675−1677.
57. Benini, S., Borsari, M., Ciurli, S., Dikiy, A., and Lamborghini, M. (1998) *J. Biol. Inorg. Chem. 3*, 371−382.
58. Benini, S., González, A., Rypniewski, W. R., Wilson, K. S., Van Beeumen, J. J., and Ciurli, S. (2000) *Biochemistry 39*, 13115−13126.
59. Scott, R. A., and Mauk, A. G. (1996) *Cytochrome c. A multidisciplinary approach*, University Science Books, Sausalito, CA.
60. Banci, L., Bertini, I., Huber, J. G., Spyroulias, G. A., and Turano, P. (1999) *J. Biol. Inorg. Chem. 4*, 21−31.
61. Koller, K. B., and Hawkridge, F. M. (1985) *J. Am. Chem. Soc. 107*, 7412−7417.
62. Marcus, R. A., and Sutin, N. (1985) *Biochim. Biophys. Acta 811*, 265−322.
63. Moore, G. R., and Pettigrew, G. W. (1990) *Cytochrome c: evolutionary, structural and physicochemical aspects*, Springer-Verlag, Berlin.
64. Rosell, F. J., Ferrer, J. C., and Mauk, A. G. (1998) *J. Am. Chem. Soc. 120*, 11234−11245.
65. Bertini, I., Banci, L., Ciurli, S., Dikiy, A., Dittmer, J., Rosato, A., Sciara, G., and Thompsett, A. (2002) *ChemBioChem 3*, 299−310.
66. Luntz, T. L., Schejter, A., Garber, E. A. E., and Margoliash, E. (1989) *Proc. Natl. Acad. Sci. U.S.A. 86*, 3424−3528.
67. Bushnell, G. W., Louie, G. V., and Brayer, G. D. (1990) *J. Mol. Biol. 214*, 585−595.
68. Berghuis, A. M., Guillemette, J. G., McLendon, G., Sherman, F., Smith, M., and Brayer, G. D. (1994) *J. Mol. Biol. 236*, 786−799.
69. Berghuis, A. M., Guillemette, J. G., Smith, M., and Brayer, G. D. (1994) *J. Mol. Biol. 235*, 1326−1341.
70. Lett, C. M., Berghuis, A. M., Frey, H. E., Lepock, E. F., and Guillemette, J. G. (1996) *J. Biol. Chem. 271*, 29088−29093.
71. Than, M. E., Hof, P., Huber, R., Bourenkov, G. P., Bartunik, H. D., Buse, G., and Soulimane, T. (1997) *J. Mol. Biol. 271*, 629−644.
72. Hasegawa, J., Yoshida, T., Yamazaki, T., Sambongi, Y., Yu, Y., Igarashi, Y., Kodama, T., Yamazaki, K., Kyogoku, Y., and Kobayashi, Y. (1998) *Biochemistry 37*, 9641−9649.
73. Allen, J. P., Feher, G., Yeates, T. O., Komiya, H., and Rees, D. C. (1987) *Proc. Natl. Acad. Sci. U.S.A. 84*, 6162−6166.
74. Tiede, D. M., Vashishta, A.-C., and Gunner, M. R. (1993) *Biochemistry 32*, 4515−4531.
75. Meyer, T. E., Bartsch, R. G., Cusanovich, M. A., and Tollin, G. (1993) *Biochemistry 32*, 4719−4726.
76. Davidson, V. L., and Jones, L. H. (1995) *Biochemistry 34*, 1238−1243.
77. Blackledge, M. J., Guerlesquin, F., and Marion, D. (1996) *Proteins: Struct., Funct., Genet. 24*, 178−194.
78. Ciurli, S., Safarov, N., Miletti, S., Dikiy, A., Christensen, S. K., Kornetzky, K., Bryant, D. A., Vandenberghe, I., Devreese, B., Samyn, B., Remaut, H., and Van Beeumen, J. J. (2002) *J. Biol. Inorg. Chem. 7*, 623−631.
79. Bertini, I., Ciurli, S., Dikiy, A., Fernandez, C., Luchinat, C., Safarov, N., Shumilin, S., and Vila, A. (2001) *J. Am. Chem. Soc. 123*, 2405−2413.
80. Hochkoeppler, A., Kofod, P., Ferro, G., and Ciurli, S. (1995) *Arch. Biochem. Biophys. 322*, 313−318.
81. Koradi, R., Billeter, M., and Wuthrich, K. (1996) *J. Mol. Graphics 14*, 51−55.

BI026473V